Journal of Hazardous Materials 187 (2011) 283–290

Contents lists available at ScienceDirect

Journal of Hazardous Materials

journal homepage: www.elsevier.com/locate/jhazmat

MnO_x–CeO_2–Al_2O_3 mixed oxides for soot oxidation: Activity and thermal stability

Xiaodong Wu*, Shuang Liu, Duan Weng, Fan Lin, Rui Ran

Laboratory of Advanced Materials, Department of Materials Science and Engineering, Tsinghua University, Beijing 100084, China

ARTICLE INFO

Article history:
Received 12 October 2010
Received in revised form
21 December 2010
Accepted 5 January 2011
Available online 12 January 2011

Keywords:
MnO_x–CeO_2 mixed oxides
Alumina modification
Diesel soot oxidation
NO oxidation
Thermal stability

ABSTRACT

MnO_x–CeO_2–Al_2O_3 mixed oxides were prepared by impregnating manganese acetate and cerium nitrate on alumina powders using the sol–gel method. The thermal stabilities of MnO_x–CeO_2 and Al_2O_3-modified mixed oxides were evaluated by treating at 800 °C in dry air flow for 20 h. The introduction of Al_2O_3 markedly increases the textural stability of the catalyst with a relatively high dispersion of MnO_x and CeO_2, remaining a strong synergistic effect between these two oxides. The NO oxidation activity of the ternary oxides experiences a smaller loss after high-temperature calcination, and a low soot oxidation temperature is attained in the presence of NO.

1. Introduction

Diesel engines have been widely used in heavy duty vehicles and for long range transport due to their fuel efficiency, reliability and durability. The removal of soot in diesel exhaust is a topic of ongoing researches due to the environmental and health impacts of these carbon nanoparticles [1]. Oxidation of typical diesel engine exhaust gas to CO_2 in the uncatalysed soot filter generally occurs at around 600 °C. The use of a catalytic trap performing both filtration and catalytic combustion of soot appears to be an effective solution.

Recently, transition metals (such as cobalt, copper and iron) supported/doped ceria mixed oxides catalysts show strong soot oxidation activity via a redox-type mechanism assisted by oxygen spillover on CeO_2 or a synergistic effect between transition metal oxides and ceria [2–7]. Especially, MnO_x–CeO_2 mixed oxides have evidenced high soot oxidation activities in both excess O_2 [8,9] and NO [10,11]. The incorporation of manganese cations into the ceria lattice greatly improves the oxygen storage capacity of ceria as well as oxygen mobility on the surface of the mixed oxides. Additionally, this catalyst is advantageous not only because of its high oxidation activity for NO conversion to NO_2, but also associated with the high NO_x storage capacity at low temperatures, which can release abundant NO_2 for soot oxidation. However, this mixed oxides catalyst shows a very low thermal stability at calcination temperatures above 500 °C, wherein the catalyst undergoes severe phase separation, dramatic reduction of surface area [12] and hereby deactivation for such as NH_3-SCR reaction [13].

Alumina has been added to CeO_2–ZrO_2 (CZ) mixed oxides as promoters for three-way catalysts to produce nanocomposite materials with thermal stabilities at temperatures up to 1100 °C [14–17]. The effect of the initial interaction between CZ and Al_2O_3 may be attributed to four factors: (i) to avoid pore collapse; (ii) to restrain the segregation of CZ; (iii) to prevent the phase transformation of alumina; and (iv) to create more lattice defects in CZ. A similar effect has been reported for the thermal stability of CuO_x–CeO_2–Al_2O_3 catalyst for soot oxidation [18] and MnO_x–CeO_2–Al_2O_3 catalyst for chlorobenzene combustion [19].

In the present study, γ-Al_2O_3 was introduced to MnO_x–CeO_2 mixed oxides to investigate how beneficial its effect will be on the structural features, redox properties and therefore the soot oxidation activities of the catalyst to open opportunities for practical applications in diesel exhaust purification.

2. Experimental

2.1. Catalyst preparation

MnO_x–CeO_2 mixed oxides with a molar ratio of 15:85 were synthesized by a citric acid-aided sol–gel method as described in [11] using $Ce(NO_3)_3{\cdot}6H_2O$ (Yili, Beijing) and $C_4H_6MnO_4{\cdot}4H_2O$ (Chemical Reagents, Beijing) as the precursors. MnO_x–CeO_2–Al_2O_3 mixed oxides were prepared by a similar method with the same Mn/Ce molar ratio and a weight ratio of $(Mn_2O_3 + CeO_2)$:Al_2O_3 = 2:1. Cerium nitrate and manganese acetate were dissolved in deionized

* Corresponding author. Tel.: +86 10 62792375; fax: +86 10 62772726.
E-mail address: wuxiaodong@tsinghua.edu.cn (X. Wu).

0304-3894/$ – see front matter © 2011 Elsevier B.V. All rights reserved.
doi:10.1016/j.jhazmat.2011.01.010

water and mixed with γ-Al_2O_3 powders (BASF, 150 m^2/g). Citric acid was added as the complexing agent with twice as the metal ions including Ce^{3+} and Mn^{2+}. Polyglycol was then added at 10% of the weight of citric acid. The solution was sufficiently stirred and heated at 80 °C until a porous gel was formed. The gel was dried at 110 °C overnight followed by decomposition at 300 °C for 1 h and calcination at 500 °C for 5 h under static air in a muffle. Both the MnO_x–CeO_2 and MnO_x–CeO_2–Al_2O_3 powders were treated at 800 °C for 20 h in a dry air flow to obtain the aged catalysts with a suffix of "-A".

2.2. Catalyst characterization

The powder X-ray diffraction (XRD) patterns were determined by a Japan Science D/max-RB diffractometer employing Cu Kα radiation (λ = 0.15418 nm). The X-ray tube was operated at 40 kV and 30 mA. The X-ray diffractograms were recorded at 0.02° intervals in the range of $20° \le 2\theta \le 80°$ with a scanning velocity of 4°/min. The lattice constants and mean crystallite sizes of ceria in the samples were calculated from Cohen's method and the Williamson–Hall equation, respectively.

The specific surface areas of the samples were measured using the N_2 adsorption isotherm at −196 °C by the four-point Brunauer–Emmett–Teller (BET) method using an automatic surface analyzer (F-Sorb 3400, Gold APP Instrument). The samples were degassed at 200 °C for 2 h prior to the measurements.

The Raman spectra were obtained with a LabRAM HR 800 (HORIBA Jobin Yvon, France) spectrometer at room temperature (RT) and atmospheric pressure. An argon ion laser beam with the wave length of 633 nm was focused on a spot of 1 μm in diameter.

The H_2 temperature-programmed reduction (TPR) tests were carried out in a fixed-bed reactor with the effluent gases monitored by a mass spectrometer (OmniStar TM). Fifty milligrams of the sample was diluted with 150 mg of silica pellets and sandwiched by quartz wool in a tubular quartz reactor. The reactor temperature was raised up to 900 °C at a heating rate of 10 °C/min in 5% H_2/He (50 ml/min).

The NO temperature-programmed oxidation (TPO) tests were carried out in a fixed-bed reactor with the effluent gases monitored by an infrared spectrometer (Thermo Nicolet 380). One hundred milligrams of catalyst powders were diluted with 300 mg of silica pellets, and then were sandwiched by quartz wool in a tubular quartz reactor. A gas mixture of 1000 ppm NO/10% O_2/N_2 was fed at a flow rate of 500 ml/min. The reactor temperature was ramped to 650 °C at a heating rate of 10 °C/min.

The NO_x temperature-programmed desorption (TPD) tests were performed in the same apparatus to that used in NO-TPO tests. Prior to the test, the sample powders were exposed in 1000 ppm NO/10% O_2/N_2 (500 ml/min) from room temperature (RT) to 300 °C at a heating rate of 10 °C/min, cooled down to RT in the same atmosphere and flushed by N_2. Afterwards, the NO and NO_2 desorption profiles were obtained by ramping the reactor from RT to 600 °C at a heating rate of 10 °C/min in a 10% O_2/N_2 stream.

2.3. Activity measurement

Printex-U (Degussa) was used as a model soot. Its particle size was 25 nm and the specific surface area was 100 m^2/g. Ten milligrams of soot and 100 mg of catalyst powders were mixed by a spatula for 2 min for "loose contact" conditions. In order to prevent reaction runaway, 110 mg of the soot–catalyst mixture was diluted with 300 mg of silica pellets. The inlet gas mixture was 10% O_2/N_2 or 1000 ppm NO/10% O_2/N_2 with a total flow rate of 500 ml/min. The activities of the catalysts for soot oxidation were evaluated in a temperature-programmed oxidation (TPO) reaction apparatus.

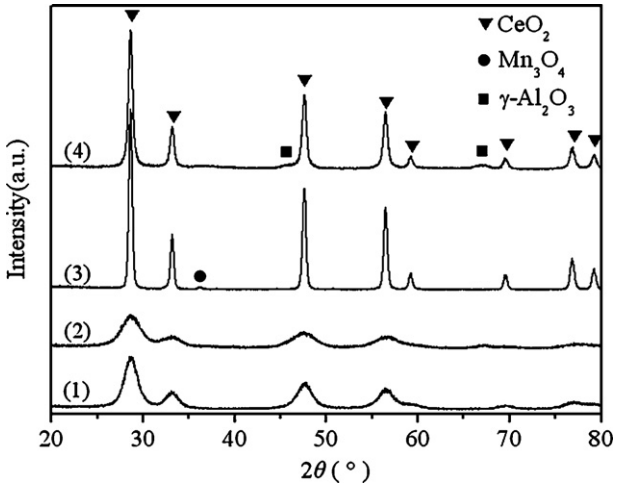

Fig. 1. XRD patterns of the (1) MnCe, (2) MnCeAl, (3) MnCe-A and (4) MnCeAl-A catalysts.

The activities of the catalysts for soot oxidation were evaluated in the same apparatus to that used in NO-TPO tests. T_m represented the maximal soot oxidation rate temperature. The downstream $CO_2/(CO_2 + CO)$ ratio during soot oxidation was defined as the selectivity to CO_2 (S_{CO_2}).

3. Results

3.1. Solid properties

The powder XRD patterns of the fresh and aged catalysts are shown in Fig. 1, and the calculated cell parameters are listed in Table 1. The fresh samples display only typical diffraction peaks of a fluorite-like structure with a smaller lattice constant (0.5395–0.5396 nm) in comparison with that of pure ceria (generally 0.5417–0.5418 nm) [9,11]. Replacement of Ce^{x+} by Mn^{x+} in the fluorite structure would decrease the lattice constant owing to the smaller ionic radii of Mn^{x+} (Mn^{4+}: 0.053 nm; Mn^{3+}: 0.065 nm; Mn^{2+}: 0.083 nm) compared with those of Ce^{x+} (Ce^{4+}: 0.097 nm; Ce^{3+}: 0.114 nm). The solubility limitation of Mn cations in CeO_2 is reported to be 5–10 mol.% depending highly on the preparation procedure [20], which is lower than the nominal Mn content in this study (15 mol.%). Meanwhile, no diffraction peaks of manganese oxides are observed for the fresh samples. Thus, it is reasonable to suggest that there are at least two kinds of Mn species in the fresh catalysts, i.e. Mn cations in the ceria lattice and highly dispersed MnO_x clusters on the surface of CeO_2 and/or Al_2O_3 [9]. The γ-Al_2O_3 support exhibits two broad diffraction peaks at $2\theta = 45.8°$ and 67.0° that are ascribed to a spinel phase. It is difficult for Al_2O_3 to enter into the ceria based solid solutions since the alumina powders were adopted as the precursor.

A typical peak of tetragonal Mn_3O_4 appears at $2\theta = 36.1°$ in the diffraction pattern of MnCe-A since Mn_3O_4 is the sole composition in various MnO_x that tolerates reversible oxygenation–deoxygenation processes at 500–1050 °C [21]. This, as well as the increase of the ceria lattice constant, indicates the

Table 1
Structural features of the catalysts.

Sample	d (nm)	D (nm)	S_{BET} (m^2/g)
MnCe	0.5395	5.9	18
MnCeAl	0.5396	4.5	130
MnCe-A	0.5406	17.9	<1
MnCeAl-A	0.5405	13.9	45

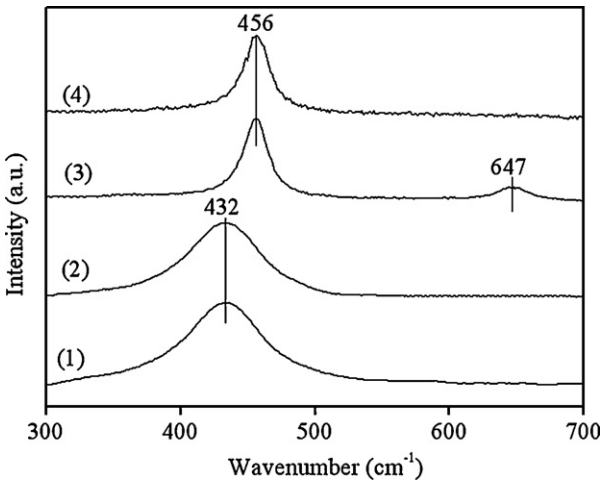

Fig. 2. Raman spectra of the (1) MnCe, (2) MnCeAl, (3) MnCe-A and (4) MnCeAl-A catalysts.

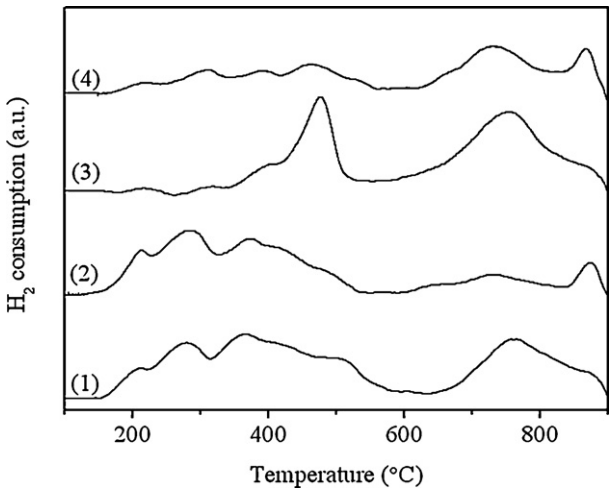

Fig. 3. H_2-TPR profiles of the (1) MnCe, (2) MnCeAl, (3) MnCe-A and (4) MnCeAl-A catalysts. Reactant gas: 5% H_2/He.

phase separation of MnO_x–CeO_2 solid solutions and the formation of bulk Mn_3O_4 after aging. On the other hand, no crystalline Mn_3O_4 is found on MnCeAl-A. The Mn species are supposed to segregate out of CeO_2 and form fine oxides with poor crystallinity since a similar increase of the ceria lattice constant occurs. MnO_x can interact with Al_2O_3 to produce Mn_2AlO_4 spinel at temperatures above 950 °C [22]. Thus, it is difficult to form such a spinel phase on the alumina-modified sample. No typical peak at 23.5° assigned to crystalline $CeAlO_3$ (1 0 0) is observed. However, the formation of some dispersed $CeAlO_3$ at the Ce–Al interface, which has been reported to prevent the formation of α-Al_2O_3 [23], cannot be excluded.

The structural features of the fresh and aged samples were confirmed by Raman spectroscopy, which is a suitable technique sensitive to M–O bond arrangements. As shown in Fig. 2, a typical band is observed at 432 cm^{-1} in the spectra of both fresh samples. It is assigned to the F_{2g} symmetric O–Ce–O stretching vibration of the fluorite–type structure and shifts towards lower wavenumbers with respect to that in CeO_2 (generally ca. 463 cm^{-1}) due to the generation of a solid solution phase of MnO_x–CeO_2 [24]. This band shifts back to 456 cm^{-1} for both aged samples ascribed to the phase separation of the solid solutions after aging. Another band appearing at 647 cm^{-1} on MnCe-A is assigned to the symmetric stretch of Mn_3O_4 groups [25], which is not found on MnCeAl-A because manganese oxides exist mainly in the form of finely dispersed clusters. These observations agree with the XRD results. It should be noted that the band at 432 cm^{-1} is also collected in the Raman spectra of the aged samples (not shown), suggesting that not all the MnO_x–CeO_2 solid solutions separate even after the high-temperature calcination.

As discussed above, the introduction of alumina does not appear to be effective in preventing the phase separation of MnO_x–CeO_2 solid solutions at high temperatures. On the other hand, the contact between (Mn,Ce)O_2 primary particles is restricted by mixing with the Al_2O_3 powders so that to some extent the growth of the oxide particles is inhibited. As shown in Table 1, the mean crystallite size of ceria in MnCeAl-A is smaller than that in MnCe-A. The introduction of alumina also succeeds in retarding the sintering of Mn_3O_4 as evidenced by the XRD and Raman results. These, as well as the contribution of the high-surface-area support, help maintain the catalyst with relatively high dispersions of CeO_2 and MnO_x which are important for soot oxidation. It has been reported that the transformation of γ-Al_2O_3 into the δ phase starts at 800 °C [15]. However, no phase transformaition of alumina is observed in this work after a 20 h calcination, suggesting a similar stabilizing effect of MnO_x–CeO_2 on the phase transformation of γ-Al_2O_3. Thus, it is plausible that the (Mn,Ce)O_2 and Al_2O_3 are well mixed at the nanometer level and can serve as diffusion barriers to each other.

3.2. H_2-TPR

The H_2-TPR profiles are shown in Fig. 3 to describe the redox property of the catalysts. MnCe shows five distinct peaks at ca. 210, 280, 365, 415 and 510 °C, which corroborate the previous reports [26,27]. The assignment of these peaks to different MnO_x species or to specific reduction steps is not straightforward because they are not only related to the oxidation state but also to the crystallinity of manganese oxides [12,28,29]. Nevertheless, it is proposed in combination with structural characterizations that the first two reduction peaks at 210 and 280 °C are related to the successive reduction of readily reducible manganese species in the solid solutions or in the form of highly dispersed MnO_x clusters. The next two overlapped reduction peaks at 365 and 415 °C correspond to the typical two-step reduction process of larger MnO_2/Mn_2O_3 crystallites. The first step involves the reduction of MnO_2/Mn_2O_3 → Mn_3O_4, and the second step represents the reduction of Mn_3O_4 → MnO. The peak at 510 °C is assigned to the reduction of Ce^{4+} → Ce^{3+} in the solid solutions. In the high-temperature region, the peaks at 760 and 870 °C are associated with the reduction of bulk ceria promoted by the adjacent MnO_x species and unpromoted bulk ceria, respectively. Similar reduction peaks are found on the alumina-modified mixed oxides. It is noted that the high-temperature reduction peak at 730 °C is weakened and that the low-temperature reduction peaks are comparable in intensity with those for MnCe, implying a strong synergistic effect between finely dispersed MnO_x and CeO_2 clusters on the surface of alumina. However, there are still some ceria powders which are not adjacent to manganese oxides due to the obstruction of alumina, resulting in a distinct reduction peak of bulk ceria at 870 °C.

It has been reported that Mn is mainly in the +3 oxidation state due to their better size compatibility with Ce^{4+} compared with Mn^{4+} [30]. The presence of a thin layer of Mn^{4+} ions on the ceria-based oxide surface must be also considered due to the well-known oxygen mobility in ceria [31]. The high dispersion of Mn^{x+} species facilitates the surface reduction of CeO_2 to low temperatures, which is critical to low-temperature H_2 consumption. The calculated low-temperature (<400 °C) H_2 consumption of MnCeAl (0.69 mmol H_2/g cat.) is close to that of MnCe (0.67 mmol H_2/g cat.). These values are obviously higher than the theoretical H_2 con-

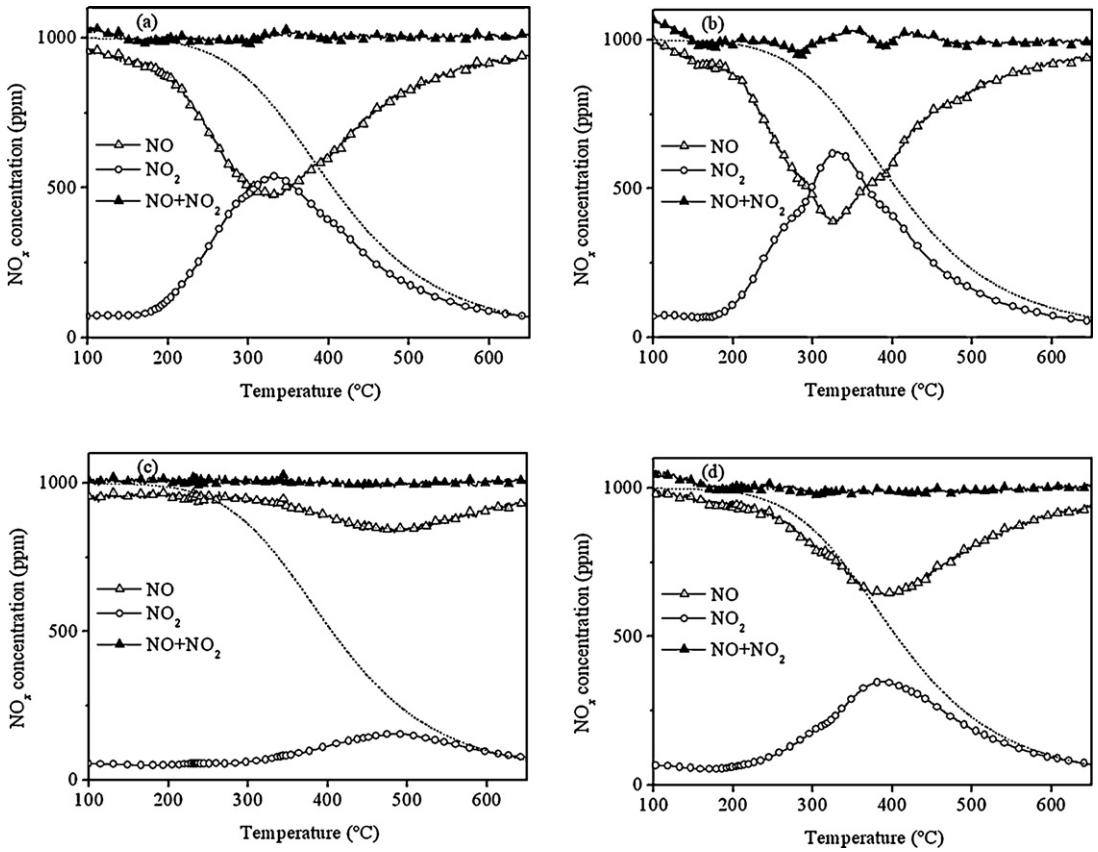

Fig. 4. NO-TPO curves of the fresh (a) MnCe, (b) MnCeAl, (c) MnCe-A and (d) MnCeAl-A catalysts. Reactant gas: 1000 ppm NO/10% O_2/N_2. The dotted line represents the NO_2 profile predicted by the thermodynamic equilibrium of the reaction $NO + (1/2)O_2 \leftrightarrow NO_2$.

sumption by reduction of Mn^{x+} in MnCe (0.24 mmol H_2/g cat.) and MnCeAl (0.16 mmol H_2/g cat.) by assuming manganese in Mn_2O_3. Thus, the concomitant reduction of ceria in the solid solutions and in the proximity of manganese oxides at low temperatures is important due to the strong synergetic effect between these two oxides [26]. A partial reduction of ceria is also during copper reduction in Cu–Ce–Al mixed oxides by a spillover process [32]. The amount of H_2 consumption depends on the extent of the incorporation of Mn species into the ceria structure and the dispersion of individual oxides, which in turn influence the surface properties of the catalysts. Therefore, the similar low-temperature redox properties between two fresh samples demonstrate higher dispersions of MnO_x and CeO_2 and their stronger synergistic effect on the surface of Al_2O_3, since the content of the reducible components in MnCeAl is only two thirds of that in MnCe.

As indicated by the XRD and Raman results, high-temperature calcination leads to a distinct separation of MnO_x–CeO_2 solid solutions and severe sintering of the oxide crystallites in MnCe-A. The low-temperature redox property of the catalyst is greatly affected due to the weakened synergistic effect between MnO_x and CeO_2. The peaks assigned to the reduction of readily reducible MnO_x species almost disappear, and those of MnO_x crystallites shift to higher temperatures due to the sintering of Mn_3O_4, with a shoulder at 400 °C assigned to the reduction of bulk $MnO_2/Mn_2O_3 \rightarrow Mn_3O_4$ and a strong peak at 475 °C to the reduction of bulk Mn_3O_4 to MnO and surface ceria. For MnCeAl-A, the low-temperature reduction peaks decrease in intensity rather than disappear, and the reduction peak of bulk ceria promoted by adjacent Mn species is enlarged. That is, at least part of MnO_x and CeO_2 remain fairly dispersed on the surface of Al_2O_3 accompanied with a rather strong synergistic effect between the oxides. Consequently, it can be said that this alumina-modified catalyst maintains a higher thermal stability in redox property than pure MnO_x–CeO_2 mixed oxides.

3.3. NO oxidation and NO_x adsorption

NO_2 production performance is critical to soot catalytic oxidation in the presence of NO. Fig. 4 shows the evolutions of NO, NO_2 and NO_x ($NO + NO_2$) during the NO-TPO measurements in the presence of 1000 ppm NO and 10% O_2. MnCe and MnCeAl exhibit an onset temperature at ca. 180 °C and a maximal NO conversion temperature at ca. 330 °C, revealing a remarkable activity for NO oxidation and similar total NO_2 production (2.74 and 2.72 mmol NO_2/g cat.). As predicted by the redox property of the aged catalysts, MnCe-A shows a much poorer activity for NO oxidation than MnCeAl-A. The total amount of NO_2 production is 1.10 and 1.88 mmol/g cat. for MnCe-A and MnCeAl-A, respectively. In addition, the effect of the thermal aging treatment is more pronounced on MnCe-A for the shift of the NO_2 production window to higher temperatures. The introduction of the high-surface-area support provides the aged catalyst with more readily available active oxygen for NO oxidation especially at low temperatures, which correlates well with the H_2-TPR curves.

The convex peak at 330 °C in Fig. 4b is suggested to partially arise from decomposition of the surface nitrates which contribute to NO_2 production at low temperatures for MnCeAl. To confirm this point, the NO_x desorption behaviors were investigated by means of TPD. The catalysts were exposed to a flow of 1000 ppm NO/10% O_2/N_2 from RT to 300 °C and were then cooled down to RT prior to the TPD tests. In an O_2-rich atmosphere, the major desorbed NO_x species is NO_2, and little NO is released from the catalysts (not shown). As shown in Fig. 5, two NO_2 desorption peaks are observed at 155 and

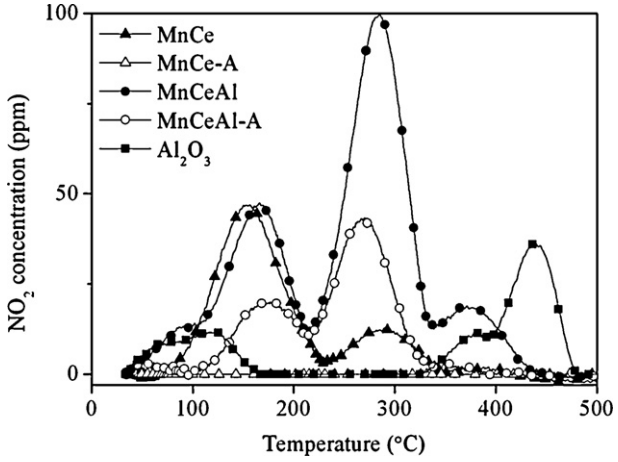

Fig. 5. NO_2-TPD profiles of the catalysts and the Al_2O_3 support. The samples were pretreated in 1000 ppm NO/10% O_2/N_2 from RT to 300 °C and then cooled down to RT.

290 °C on MnCe ascribed to the desorption of weakly adsorbed NO_2 and the decomposition of bidentate/monodentate nitrates, respectively [27]. The second peak becomes much stronger on MnCeAl, which demonstrates the importance of the high-surface-area support on the formation of nitrates coordinated to Mn^{x+} and Ce^{x+} sites. The support itself also contributes to the nitrate storage capacity of MnCeAl, with two NO_2 desorption peaks at 95 and 370 °C, which are ascribed to desorption of weakly adsorbed NO_2 and bidentate/monodentate/bridged aluminum nitrates, respectively [33]. After the aging treatment, almost no NO_2 is desorbed from MnCe-A, while two weakened NO_2 desorption peaks at 175 and 270 °C remain on the aged alumina-modified catalyst. The amounts of NO_2 desorbed from MnCe, MnCeAl, MnCeAl-A and Al_2O_3 were estimated to be 0.10, 0.26, 0.10 and 0.07 mmol/g cat., respectively. The extra low surface area and severe sintering of oxide crystallites are responsible for the complete loss of NO_x storage capacity in MnCe-A.

3.4. Soot-TPO

The evolutions of CO_x (CO and CO_2) and NO_x ($NO + NO_2$) were recorded during the soot-TPO measurements in $NO + O_2$ and O_2. Table 2 lists the maximal soot oxidation rate temperature (T_m) and the selectivity to CO_2 (S_{CO_2}) of the catalysts. For comparison, the uncatalysed data obtained from the blank test and those from the catalysed reactions are also given in the table. The table shows that the complete oxidation of soot is dominant for both fresh catalysts and MnCeAl-A, while the CO_2 selectivity of MnCe-A is close to that of the uncatalysed reaction. The presence of NO_x in the reaction atmosphere promotes the catalytic oxidation of soot. Both fresh catalysts exhibit high activities for NO_2-assisted soot oxidation with the T_m around 450 °C. The T_m of MnCe-A (554 °C) is lower than that in the uncatalysed reaction (610 °C), indicating that this aged catalyst still works in the presence of NO_x even if it experiences a striking deactivation. On the other hand, the T_m of the alumina-modified MnO_x–CeO_2 mixed oxides shifts upwards by 53 °C after a long high-temperature calcination.

Table 2
Soot oxidation activities of the catalysts.

Catalyst	In $NO + O_2$		In O_2		ΔT_m (°C)
	T_m (°C)	S_{CO_2} (%)	T_m (°C)	S_{CO_2} (%)	
MnCe	448	98	535	99	87
MnCeAl	455	98	575	98	120
MnCe-A	554	51	598	61	45
MnCeAl-A	508	90	590	94	82
Uncatalysed	610	45	612	47	2

Fig. 6 shows the soot-TPO curves in the presence of NO and O_2 to explore possible relationships between CO_x production and NO_2 consumption. Taking Fig. 6b as an example, the low-temperature NO_x peak (<170 °C) is ascribed to the desorption of weakly adsorbed NO. NO_2 is detected from 200 °C and reaches a maximal concentration at 330 °C. As indicated by the NO_x-TPD results, the stored NO_x desorbs mainly in the form of NO_2. However, the nitrate-derived NO_2 is not as important as expected at a high gas flow rate of 1 L/min and in a diluted soot–catalyst reaction without obvious heat transfer limitations [11]. The NO_2 gap between NO- and soot-TPO runs may be generated from consumption of NO_2 by reaction with soot. It is noted that the NO_2 consumption at 330 °C (ca. 200 ppm) is less than the CO_2 production (ca. 300 ppm) on MnCeAl. One reason is that the reduced NO is recycled to NO_2. This reoxidized NO_2, in turn, can participate in the soot oxidation again. The NO_2 gaps between two runs are larger on the aged catalysts, which also demonstrate the decreased recycling efficiency of $NO \leftrightarrow NO_2$ after aging. Another possible explanation is that not only NO_2 but also O_2 is involved in the initial oxidation of soot. The activation energy (E_a) for soot oxidation were calculated from the least square fit of the data drawn in a 10–50% soot conversion range according to the Arrhenius plots, and the results are 79, 80, 100 and 86 kJ/mol for MnCe, MnCeAl, MnCe-A and MnCeAl-A, respectively. The corresponding E_a values by running the soot-TPO with the fresh catalysts in 10% O_2/N_2 and 2000 ppm NO_2/N_2 are around 150 and 50 kJ/mol, respectively. Thus, it confirms that both NO_2 and O_2 participate in the first half stage of soot oxidation, and the contribution of O_2 becomes predominant for MnCe-A with which the produced NO_2 is almost completely consumed by reaction with soot. We have described the "trigger" effect of NO_2 on soot oxidation in our previous studies [11,27], which also applies here. As shown in Fig. 6, the NO_2 utilization efficiency is high on the fresh catalysts and MnCeAl-A. This indicates that the soot oxidation is not limited by NO_2 production with these catalysts, whereas it is obviously restricted to a great extent by the rate of NO conversion to NO_2 over MnCe-A. With the successive oxidation of soot, the NO_2 concentration decreases and the extensive oxidation of soot by O_2 becomes dominant. The NO_2 concentration begins to increase back to original levels as in the NO-TPO runs when the temperature reaches the T_m for soot oxidation. These facts support that the oxidation of soot by NO_2 is still involved in this stage although it is less important. It is interesting to note that the NO_x concentration can decrease to about 930–940 ppm during the first half stage of soot oxidation with all the catalysts, suggesting that NO_2 itself is reduced to NO and even N_2 to a limited extent by reaction with soot.

4. Discussion

4.1. Relationship between redox property and soot oxidation activity

The redox property of the catalyst, which is characterized by H_2-TPR measurement, is suggested to be essential for soot oxidation activities in both NO-free and NO-containing atmospheres. As shown in Fig. 7a, the total amount of hydrogen consumption from RT to 900 °C follows the order of MnCe > MnCe-A > MnCeAl > MnCeAl-A. The amount of available oxygen from the alumina-modified mixed oxides is weakened due to the addition of the inert support. It is clear that these data are not in line with the soot oxidation activities in the presence of O_2 especially for the aged catalysts. The H_2 consumption below 600 °C is chosen as an indicator of redox property since the soot oxidation is completed around

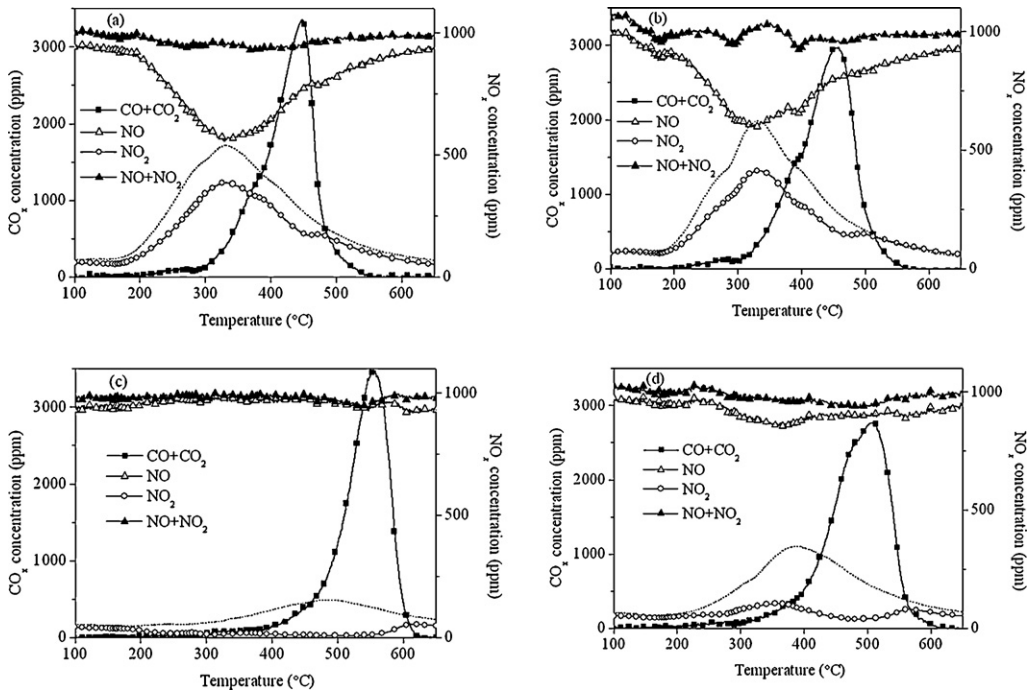

Fig. 6. Soot-TPO curves of the fresh (a) MnCe, (b) MnCeAl, (c) MnCe-A and (d) MnCeAl-A catalysts. Catalyst = 100 mg, soot = 10 mg, loose contact conditions, reactant gas: 1000 ppm NO/10% O_2/N_2. The dotted line represents the NO_2 profile in the NO-TPO measurements.

this temperature over all the catalysts. A good aggrement is established between the low-temperature H_2 consumption (<600 °C) and soot oxidation activity in the presence of oxygen, indicating the importance of active oxygen species from the MnO_x–CeO_2 mixed oxides framework. Similarly, considering that the onset of soot oxidation generally takes place around 300–400 °C, the redox property of the catalyst at lower temperatures (<400 °C) is associated with the soot oxidation activity in NO + O_2 even if these two reactions are intrinsically different. Again, a fine consistency is found among the low-temperature H_2 consumption (<400 °C), the low-temperature NO_2 production (<400 °C) and soot oxidation activity in the presence of NO + O_2 as shown in Fig. 7b. It is known that NO_2 plays an important role in soot oxidation, and the low-temperature NO oxidation activity of the catalysts does follow a sequence similar to the catalyst redox property. The specific testing conditions (such as the amount of catalyst and concentration of reactants) and reaction mechanisms may account for the higher level of NO_2 production in relation to H_2 consumption.

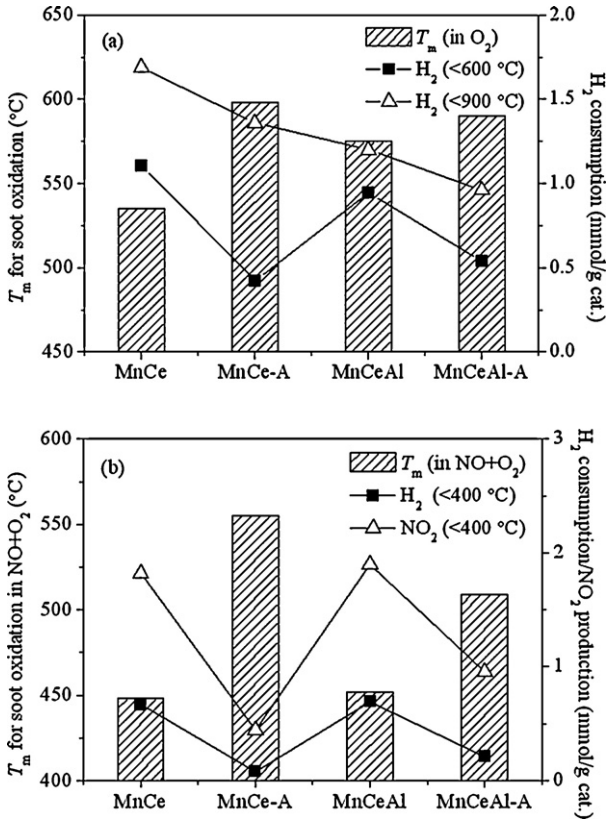

Fig. 7. Relationship between the redox property and soot oxidation activity of catalysts in (a) O_2 and (b) NO + O_2.

4.2. Relationship between NO oxidation and soot oxidation activities

In our previous study [27], the soot oxidation activity of Ba/MnO_x–CeO_2 catalysts under a heat transfer limitation can be linearly associated to the amount of NO_x releasable within 350–400 °C. Considering that no barium species is used as a NO_x storage component and the catalyst–soot mixture was diluted with silica pellets to prevent reaction runaway in this study, the importance of the nitrates stored on the catalyst is weakened to a large degree. If we compare the amounts of the NO-derived NO_2 (Fig. 4) with those of the nitrate-derived NO_2 (Fig. 5), the latter are obviously fewer. Therefore, the soot oxidation activities of MnO_x–CeO_2 based catalysts in the presence of NO_x are related to the NO_2 production behaviors in NO-TPO measurements, and the results are shown in Fig. 8.

A linear relationship between the NO_2 production at low temperatures (<400 °C) and T_m for soot oxidation is seen in Fig. 8a. Low-temperature NO_2 production for MnCeAl-A (0.96 mmol/g cat.) is more than twice of that for MnCe-A (0.44 mmol/g cat.). This explains the relatively higher soot oxidation activity of the alumina-modified catalyst after aging and demonstrates the importance of

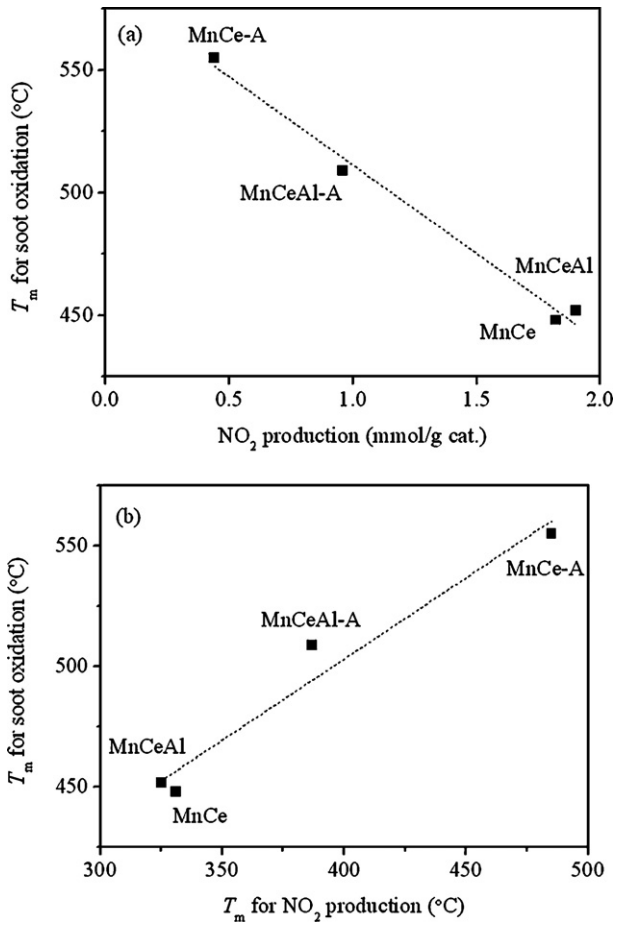

Fig. 8. (a) NO_2 production (<400 °C) and (b) its T_m versus T_m for soot oxidation with different catalysts in NO + O_2.

NO_2 for soot catalytic oxidation. Although a little more NO_2 is produced at low temperatures on MnCeAl (1.90 mmol NO_2/g cat.) with respect to MnCe (1.82 mmol NO_2/g cat.)—which may be associated to the higher NO_x storage capacity—the alumina-modified catalyst exhibits a slightly higher T_m. Again, this corroborates that the contribution from the nitrate-derived NO_2 is less important in this case.

The maximal NO_2 production temperature is considered as another factor that affects the soot oxidation activity [34]. It is important for NO_2 production to occur within the required temperature interval in which soot oxidation can be effectively promoted by NO_2. Again, the match between the two T_m values demonstrates the role of NO_2 in soot oxidation. The availability of NO_2 will be limited by the thermodynamic equilibrium of the $NO + (1/2)O_2 \leftrightarrow NO_2$ reaction at high temperatures, which is the case for MnCe-A.

4.3. Effect of Al_2O_3 as a diffusion barrier

The catalyst surface area is suggested to play an important role in soot catalytic oxidation. γ-Al_2O_3 can provide high surface area for the accessibility of active sites to gaseous reactants and to the soot. A significant drop of the surface area from 130 to 45 m^2/g for MnCeAl catalyst upon ageing at 800 °C. However, the soot oxidation activity of MnO_x–CeO_2 mixed oxides is obviously affected only when the catalyst surface area is below 8 m^2/g according to our previous study [35]. In this sense, other factors such as sintering of active oxides would be more important than the surface area of MnCeAl ranged between 45 and 130 m^2/g.

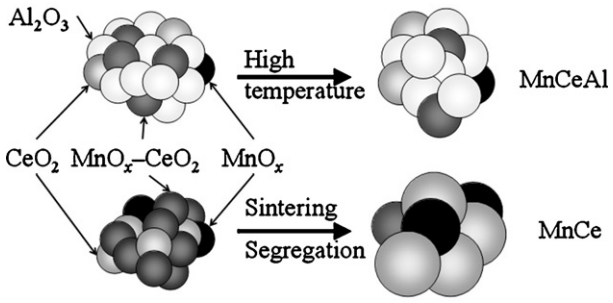

Fig. 9. Schematic diagram of introduction of Al_2O_3 as a diffusion barrier.

The growth of the mixed oxides nanoparticles would be generated through contact of the primary particles. The concept of introducing a third oxide into binary mixed oxides on a nanometer scale has been accepted as a "diffusion barrier concept" such as ACZ, i.e. a composite of alumina (A) and ceria–zirconia mixed oxides (CZ). A similar effect is achieved by introducing alumina into MnO_x–CeO_2 mixed oxides as shown in Fig. 9. No diffraction peaks of Mn_2AlO_4 or $CeAlO_3$ are obvserved on MnCeAl-A after treatment at 800 °C, as alumina does not react with (Mn,Ce)O_2 to form crystalline compounds. The contact of (Mn,Ce)O_2 primary particles is restricted and the growth of particles could be inhibited according to the XRD and Raman results. On the other hand, more MnO_x–CeO_2 solid solutions remain on the surface of alumina as indicated by H_2-TPR curves. This higher thermal stability in the textural and structural property of the ternary mixed oxides results in a superior catalytic performance of MnCeAl after aging. The T_m of MnCe and MnCeAl for soot oxidation in the presence of NO shifts to higher temperature by 106 and 53 °C after calcination at 800 °C for 20 h, respectively. It demonstrates that the addition of alumina as the support of MnCe are beneficial for practical application of the mixed oxides catalyst in diesel exhaust purification.

5. Conclusions

The MnO_x–CeO_2–Al_2O_3 mixed oxides catalyst exhibits the maximum soot oxidation rate at 455 °C, which shifts upwards by 53 °C after exposure to flow air at 800 °C for 20 h. Compared with MnO_x–CeO_2, the superior thermal stability of the Al_2O_3-modified catalyst should be mainly ascribed to retarding the sintering of MnO_x and CeO_2 crystallites as well as preventing the phase separation of MnO_x–CeO_2 solid solutions to some extent. These maintain a rather strong synergistic effect between Mn and Ce species on the nanometer scale for the aged alumina-modified catalyst, and increase the amount of available active oxygen for NO and soot oxidations at relatively low temperatures. A good accordance is found between the low-temperature redox property (<600 °C) and soot oxidation activity in O_2. A similar consistency appears between the redox property at lower temperatures (<400 °C) and soot oxidation activity in NO + O_2, where NO_2 plays an important role via the amount and the matching temperature range of its production.

Acknowledgements

The authors would like to acknowledge Project 51072096 supported by National Natural Science Foundation of China as well as Projects 2010CB732304 and 2009AA06Z313 the Ministry of Science and Technology of China.

References

[1] B. Giechaskiel, B. Alföldy, Y. Drossinos, A metric for health effects studies of diesel exhaust particles, J. Aerosol Sci. 40 (2009) 639–651.

[2] P.G. Harrison, I.K. Ball, W. Daniell, P. Lukinskas, M. Céspedes, E.E. Miró, M.A. Ulla, Cobalt catalysts for the oxidation of diesel soot particulate, Chem. Eng. J. 95 (2003) 47–55.
[3] J. Liu, Z. Zhao, J.Q. Wang, C.M. Xu, A.J. Duan, G.Y. Jiang, Q. Yang, The highly active catalysts of nanometric CeO_2-supported cobalt oxides for soot combustion, Appl. Catal. B 84 (2008) 185–195.
[4] H. Muroyama, S. Hano, T. Matsui, K. Eguchi, Catalytic soot combustion over CeO_2-based oxides, Catal. Today 153 (2010) 133–135.
[5] X.D. Wu, Q. Liang, D. Weng, Z.X. Lu, The catalytic activity of CuO–CeO_2 mixed oxides for diesel soot oxidation with a NO/O_2 mixture, Catal. Commun. 8 (2007) 2110–2114.
[6] Q. Liang, X.D. Wu, D. Weng, Z.X. Lu, Selective oxidation of soot over Cu doped ceria/ceria–zirconia catalysts, Catal. Commun. 9 (2008) 202–206.
[7] Z.L. Zhang, D. Han, S.J. Wei, Y.X. Zhang, Determination of active site densities and mechanisms for soot combustion with O_2 on Fe-doped CeO_2 mixed oxides, J. Catal. doi:10.1016/j.jcat.2010.08.017.
[8] Q. Liang, X.D. Wu, D. Weng, H.B. Xu, Oxygen activation on Cu/Mn–Ce mixed oxides and the role in diesel soot oxidation, Catal. Today 139 (2008) 113–118.
[9] W.J. Shan, N. Ma, J.L. Yang, X.W. Dong, C. Liu, L.L. Wei, Catalytic oxidation of soot particulates over MnO_x–CeO_2 oxides prepared by complexation-combustion method, J. Nat. Gas Chem. 19 (2010) 86–90.
[10] K. Tikhomirov, O. Kröcher, M. Elsener, A. Wokaun, MnO_x–CeO_2 mixed oxides for the low-temperature oxidation of diesel soot, Appl. Catal. B 64 (2006) 72–78.
[11] X.D. Wu, F. Lin, H.B. Xu, D. Weng, Effects of adsorbed and gaseous NO_x species on catalytic oxidation of diesel soot with MnO_x–CeO_2 mixed oxides, Appl. Catal. B 96 (2010) 101–109.
[12] X.F. Tang, Y.G. Li, X.M. Huang, Y.D. Xu, H.Q. Zhu, J.G. Wang, W.J. Shen, MnO_x–CeO_2 mixed oxide catalysts for complete oxidation of formaldehyde: effect of preparation method and calcination temperature, Appl. Catal. B 62 (2006) 265–273.
[13] M. Casapu, O. Kröcher, M. Elsener, Screening of doped MnO_x–CeO_2 catalysts for low-temperature NO-SCR, Appl. Catal. B 88 (2009) 413–419.
[14] J. Kašpar, P. Fornasiero, Nanostructured materials for advanced automotive depollution catalysts, J. Solid State Chem. 171 (2003) 19–29.
[15] R.D. Monte, P. Fornasiero, S. Desinan, J. Kašpar, J.M. Gatica, J.J. Calvino, E. Fonda, Thermal stabilization of $Ce_xZr_{1-x}O_2$ oxygen storage promoters by addition of Al_2O_3: effect of thermal aging on textural, structural, and morphological properties, Chem. Mater. 16 (2004) 4273–4285.
[16] J. Wang, J. Wen, M.Q. Shen, Effect of interaction between $Ce_{0.7}Zr_{0.3}O_2$ and Al_2O_3 on structural characteristics, thermal stability, and oxygen storage capacity, J. Phys. Chem. C 112 (2008) 5113–5122.
[17] A. Morikawa, T. Suzuki, T. Kanazawa, K. Kikuta, A. Suda, H. Shinjo, A new concept in high performance ceria–zirconia oxygen storage capacity material with Al_2O_3 as a diffusion barrier, Appl. Catal. B 78 (2007) 210–221.
[18] X.D. Wu, F. Lin, D. Weng, J. Li, Simultaneous removal of soot and NO over thermal stable Cu–Ce–Al mixed oxides, Catal. Commun. 9 (2008) 2428–2432.
[19] M. Wu, X.Y. Wang, Q.G. Dai, Y.X. Gu, D. Li, Low temperature catalytic combustion of chlorobenzene over Mn–Ce–O/γ-Al_2O_3 mixed oxides catalyst, Catalysis Today, doi:10.1016/j.cattod.2010.04.006.
[20] C.Y. Kang, H. Kusaba, H. Yahiro, K. Sasaki, Y. Teraoka, Preparation, characterization and electrical property of Mn-doped ceria-based oxides, Solid State Ionics 177 (2006) 1799–1802.
[21] M.I Zaki, M.A. Hasan, L. Pasupulety, K. Kumari, Thermochemistry of manganese oxides in reactive gas atmospheres: probing redox compositions in the decomposition course $MnO_2 \rightarrow MnO$, Thermochim. Acta 303 (1997) 171–181.
[22] P.G. Tsyrulnikov, S.V. Tsybulya, G.N. Kryukova, A.I. Boronin, S.V. Koscheev, T.G. Starostina, A.V. Bubnov, E.N. Kudrya, Phase transformations in the thermoactivated MnO_x–Al_2O_3 catalytic system, J. Mol. Catal. A 79 (2002) 213–220.
[23] A. Piras, A. Trovarelli, G. Dolcetti, Remarkable stabilization of transition alumina operated by ceria under reducing and redox conditions, Appl. Catal. B 28 (2000) 77–81.
[24] T. Sato, T. Komanoya, Selective oxidation of alcohols with molecular oxygen catalysed by Ru/MnO_x/CeO_2 under mild conditions, Catal. Commun. 10 (2009) 1095–1098.
[25] Y.F. Han, F.X. Chen, Z.Y. Zhong, K. Ramesh, E. Widjaja, L.W. Chen, Synthesis and characterization of Mn_3O_4 and Mn_2O_3 nanocrystals on SBA-15: novel combustion catalysts at low reaction temperatures, Catal. Commun. 7 (2006) 739–744.
[26] D. Delimaris, T. Ioannides, VOC oxidation over MnO_x–CeO_2 catalysts prepared by a combustion method, Appl. Catal. B 84 (2008) 303–312.
[27] X.D. Wu, S. Liu, F. Lin, D. Weng, Nitrate storage behavior of Ba/MnO_x–CeO_2 catalyst and its activity for soot oxidation with heat transfer limitations, J. Hazard. Mater. 181 (2010) 722–728.
[28] Z.Q. Zou, M. Meng, Y.Q. Zha, Surfactant-assisted synthesis, characterizations, and catalytic oxidation mechanisms of the mesoporous MnO_x–CeO_2 and Pd/MnO_x–CeO_2 catalysts used for CO and C_3H_8 oxidation, J. Phys. Chem. C 114 (2010) 468–477.
[29] E.R. Stobbe, B.A. de Boer, J.W. Geus, The reduction and oxidation behavior of manganese oxides, Catal. Today 47 (1999) 161–167.
[30] B. Murugan, A.V. Ramaswamy, D. Srinivas, C.S. Gopinath, V. Ramaswamy, Nature of manganese species in $Ce_{1-x}Mn_xO_{2-\delta}$ solid solutions synthesized by the solution combustion route, Chem. Mater. 17 (2005) 3983–3993.
[31] M. Casapu, O. Kröcher, M. Mehring, M. Nachtegaal, C. Borca, M. Harfouche, D. Grolimund, Characterization of Nb-containing MnO_x–CeO_2 catalyst for low-temperature selective catalytic reduction of NO with NH_3, J. Phys. Chem. C 114 (2010) 9791–9801.
[32] C. Decarne, E. Abi-Aad, B.G. Kostyuk, V.V. Lunin, A. Aboukaïs, Characterization of cerium and copper species in Cu–Ce–Al oxide systems by temperature programmed reduction and electron paramagnetic resonance, J. Mater. Sci. 39 (2004) 2349–2356.
[33] B. Westerberg, E. Fridell, A transient FTIR study of species formed during NO_x storage in the Pt/BaO/Al_2O_3 system, J. Mol. Catal. A 165 (2001) 249–263.
[34] I. Atribak, B. Azambre, A. Bueno López, A. García-García, Effect of NO_x adsorption/desorption over ceria–zirconia catalysts on the catalytic combustion of model soot, Appl. Catal. B 92 (2009) 126–137.
[35] X.D. Wu, S. Liu, D. Weng, F. Lin, Textural–structural properties and soot oxidation activity of MnO_x–CeO_2 mixed oxides, Catal. Commun. 12 (2011) 345–348.